The effect of increased axle loading on the behavior of heavily overconsolidated railway foundation materials

Mpye, G.D. (Godisang David)[1*] david.mpye@up.ac.za
Gräbe, P.J. (Petrus Johannes)[1] hannes.grabe@up.ac.za

[*]Corresponding author: Mpye, G.D. (Godisang David)

[1]Department of Civil Engineering, University of Pretoria, Lynnwood Road, Hatfield, Pretoria, Gauteng, South Africa, 0002.

ABSTRACT: The benefits of increased axle loading in the railway industry are well-appreciated to such an extent that increased axle loading has become a themed topic of interest across all disciplines of railway engineering. However, it remains important to understand the engineering behavior and performance of each track component under increased axle loading. This study was particularly interested in the behavior of railway foundation materials under increased axle loading, starting from a base load of 20 tonnes per axle for general freight to increased loads of 26, 30, 32.5 and 40 tonnes per axle for heavy haul. The methodology followed involved formulation of a theoretical model for analyses, characterization of the cyclic railway loading via finite element modelling, experimental laboratory work using a cyclic triaxial apparatus followed by detailed analyses, interpretation and discussion of the test results.

Based on the test results from the monotonic and cyclic loading, it was found that the critical state line was related to the various phase transitions in soil behavior and the resilient strain was found to be inversely related to the permanent strain. Stress states slightly above the critical state line resulted in a double-phase transition in soil behavior from dilation to contraction and then work softening with cyclic mobility. Stress states on the critical state line resulted in a single-phase transition in soil behavior from dilation to contraction with a combination of cyclic mobility and shakedown. Stress states below the critical state line resulted in a no-phase transition in soil behavior accompanied by dilation with shakedown. In relation to the effect of increased axle loading on saturated heavily overconsolidated railway materials, it was therefore concluded that resilience can be characterized by a no-phase transition predominated by linear permanent deformations and shakedown behavior while failure is characterized by a double-phase transition predominated by exponential permanent deformations and cyclic mobility behavior.

KEYWORDS increased axle loading; railway foundation materials; cyclic loading; critical state line; phase transition.

1. INTRODUCTION

According to Li et al. (2016), both developed and developing countries including Australia, Brazil, Canada, China, South Africa, Sweden and the United States of America strive towards moving heavy freight from road to the rail as part of their sustainability policies on transportation. This has inherently led to increased axle loading being implemented on existing and new railways, because the operations of heavy haul freight trains become more sustainable and feasible at increased axle loading resulting in maximum payload per train, which harnesses the benefits of economies-of-scale. In line with a white paper drafted by the European Commission, Korpanec et al. (2005) stated that increased axle loading to between 25 and 35 tonnes per axle is profitable for the transportation of bulk freight. According to Hay (1982) and Cole (2006), the Davis equation showed that the rolling resistance between the wheel-rail interface is inversely proportional to the axle loading, which leads to efficient energy consumption. It therefore remains crucially important to understand the engineering behavior and performance of each railway track component, particularly the subballast and subgrade layers in the foundation substructure as they are designed to be maintenance-free throughout the lifecycle of the track structure.

Numerous research work towards understanding the behavior of railway foundation materials under heavy haul loading has been published. Gräbe (2002) and Gräbe and Clayton (2009; 2014) focused on the effect of principal stress rotation using a hollow cylinder triaxial apparatus at a fixed axle loading of 26 tonnes per axle. Powrie et al. (2007) modelled the stress changes within the railway foundation layers at a fixed load of 25.4 tonnes per axle using finite element analysis. Priest et al. (2010) presented field measurements of transient ground movement of a railway foundation at a fixed maximum loading of 26 tonnes per axle. A pioneering study was done by the ORE (1987) on the effect of increased axle loading from 20 to 22.5 tonnes per axle on the increase of track maintenance costs. Korpance et al. (2005) gave a generalized analysis on the influencing parameters of increased axle loading from 22.5 to 26 and 30 tonnes per axle. Li and Selig (1994; 1996; 1998a; 1998b) undertook a series of studies and developed an analytical foundation design methodology based on linear elastic theory. To date, very little advanced research work, specifically linking increased axle loading with principles of critical state soil mechanics has been published.

The objective of this study was to investigate the effect of increased axle loading on the behavior of railway foundation materials. The considered axle loading cases were 20, 26, 30, 32.5 and 40 tonnes per axle, of which 20 tonnes per axle represented the general freight standards and those greater than 25 tonnes per axle represented the heavy-haul standards as stipulated by the by-laws of the International Heavy Haul Association (IHHA). In order to achieve this objective, materials which were representative of railway foundation materials were used as test materials in the laboratory using a cyclic triaxial apparatus for the experimental work. An elasto-plastic state boundary model which incorporate

principles of critical state soil mechanics was adopted for analysis of the soil behavior and the resultant resilient and permanent strains were studied in detail, proceeded by discussion of the results and formulation of conclusions.

2. RAILWAY TRACK FOUNDATION STRUCTURE

A conventional ballast railway track structure is shown in Figure 1. Each component is important and fulfils the required performance and functions as described by Selig and Waters (1994). The conventional track structure consists mainly of the superstructure and the substructure. The superstructure consists of the rails, fastening systems, pads, sleepers and crib ballast. The substructure consists of the ballast, subballast and subgrade. The subballast is the layer of aggregate between the ballast and subgrade interface. According to Selig and Waters (1994), older railway tracks did not have a subballast layer and its incorporation reduces the otherwise required greater thickness of the more expensive ballast material. Apart from cost reduction, the main functions of the subballast are to reduce stresses to the underlying subgrade and to extend the subgrade protection against freezing. The subgrade is the foundation upon which the track structure is constructed. Depending on the in-situ conditions, the subgrade can be natural or imported. The main function of the subgrade is to provide a stable foundation for the subballast, ballast and superstructure. The subballast and subgrade are subjected to cyclic stresses imposed by passing trains. Furthermore, throughout the life cycle of a railway line, the subballast and subgrade are expected to perform adequately without any maintenance intervention, as maintenance will require line-closure and total construction. It therefore reinforces the need to understand the engineering behavior of foundation materials, which this study aimed to shed light on.

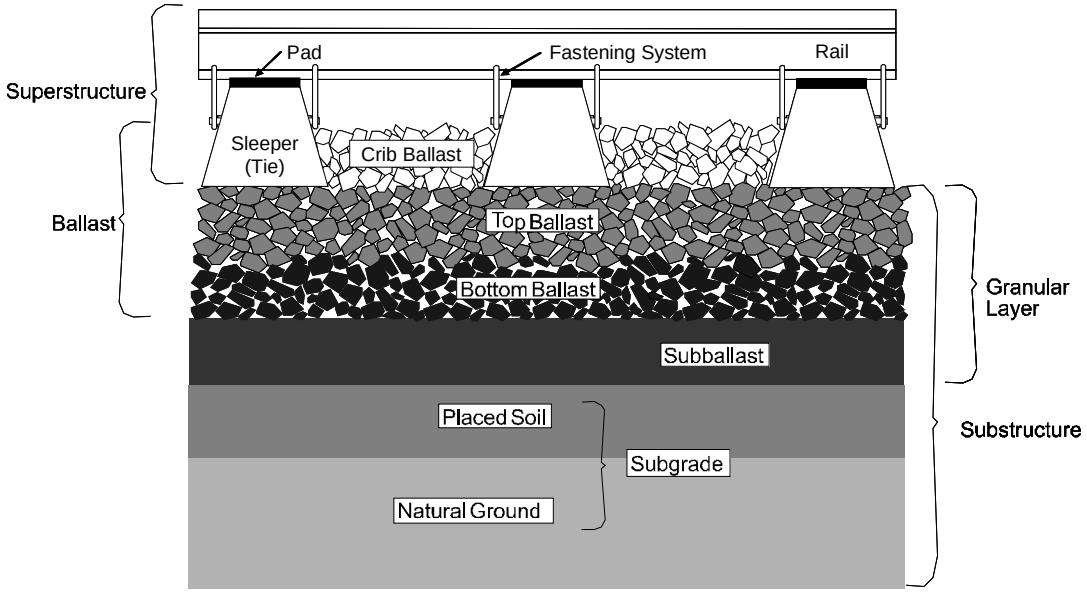

Figure 1: Conventional railway track structure (adapted from Selig and Waters (1994))

3. THEORETICAL ELASTO-PLASTIC MODEL

An elasto-plastic state boundary model has been chosen to analyze the effect of increased axle loading on the behavior of railway materials. According to various researchers including Roscoe and Burland (1968), Atkinson and Bransby (1978), Wood (1990) and Potts and Zdarkovic (1999), the realistic behavior of soil consists of elastic and plastic behavior. The elasto-plastic model shown in Figure 2 consists of the critical state line and Roscoe curve as stress state boundaries which separate elastic and plastic behavior. The elastic behavior is expected when the stress state in the soil is below the stress state boundaries. Plastic behavior is expected when the stress state in the soil is equal or greater than the stress state boundaries. The critical state line represents stress states that will result in perfectly plastic behavior, where the plastic strain increases at a constant load. Li and Selig (1996) maintained that excessive plastic deformations can be associated with failure of railway foundation materials. The critical state line (q_c) is represented by Equation (1) bounded by a domain between 0 and $p_c/2$, the Roscoe curve (q_R) is represented by Equation (2) bounded by a domain between $p_c/2$ and p_c The effective stress ratio at critical state or the slope of the critical state line (M_c) is represented by Equation (3). These stress state boundaries can therefore be viewed as failure criteria for railway foundation material during cyclic loading.

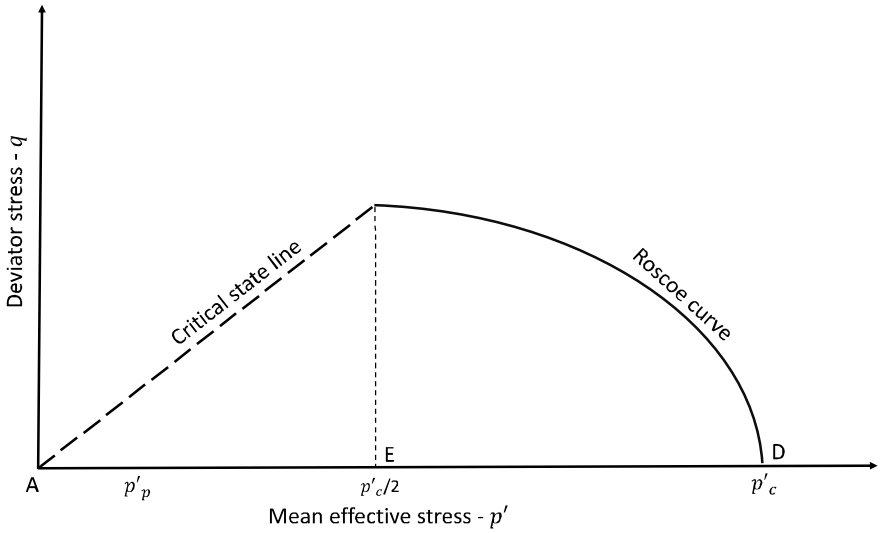

Figure 2: Elasto-plastic stress state boundary model (redrawn from Atkinson and Bransby (1978))

$$q_c = M_c p' \tag{1}$$

$$q_R = M_c \sqrt{p'\left(p'_c - p'\right)}, \tag{2}$$

$$M_c = \left(6 \sin \phi'_c\right) / \left(3 - \sin \phi'_c\right) \tag{3}$$

Where:

q_c = deviator stress of critical state line $(\sigma_1 - \sigma_3)$,

q_R = deviator stress of Roscoe curve $(\sigma_1 - \sigma_3)$,

p' = mean effective stress ($(\sigma'_1 + 2\sigma'_3)/3$),

p'_c = effective pre-consolidation pressure,

M_c = effective stress ratio at critical state,

ϕ'_c = effective angle of internal friction at critical state,

σ'_1 = effective major principle stress,

σ'_3 = effective minor principle stress.

4. CYCLIC LOADING ON A RAILWAY FOUNDATION

According to Li et al. (2016), a railway track foundation is subjected to static, cyclic and dynamic loading. The static loading is the gross mass measured in tonnes per axle. The cyclic loading, also called repeated loading, is the static loading moving at a certain speed caused by a passing train. The dynamic loading is transient in nature, arising from track and vehicle irregularities. This study focused mainly on static and cyclic loading directly related to increased axle loading. O'Reilly and Brown (1991) defined cyclic loading as a system of loading which exhibits a degree of regularity both in its magnitude and in its frequency. Li et al. (2016) went further and stated that cyclic loading is characterized by three parameters, namely, shape, magnitude and frequency. Figure 3(b) illustrates the configuration of cyclic loading on a railway track foundation in the field as a result of the moving train wheels depicted in Figure 3(a). The maximum stresses occur directly beneath the wheels and the minimum stresses occur in the middle of the wagon, which therefore need to be transformed to the configuration of cyclic loading for triaxial stress space for laboratory testing as illustrated in Figure 4 and presented in Equations (4) and (5).

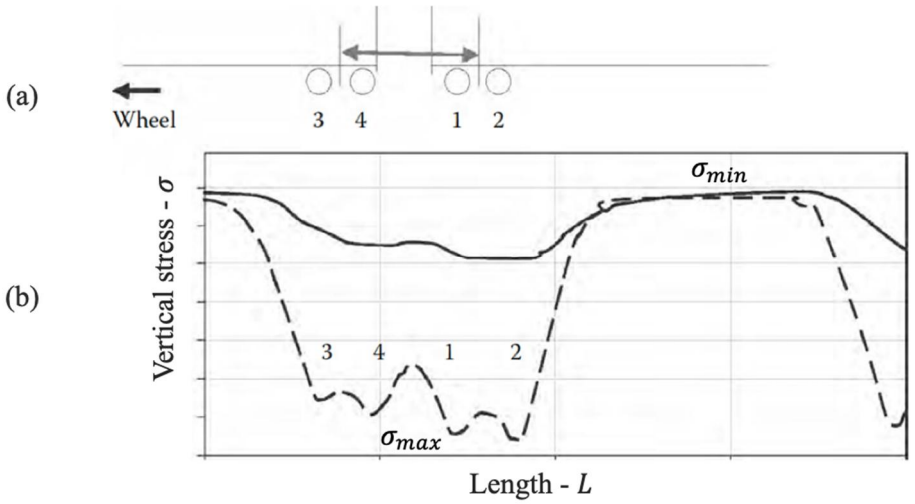

Figure 3: Cyclic loading under field conditions (a) wheel loads (b) shape (adapted from Li et al., 2016)

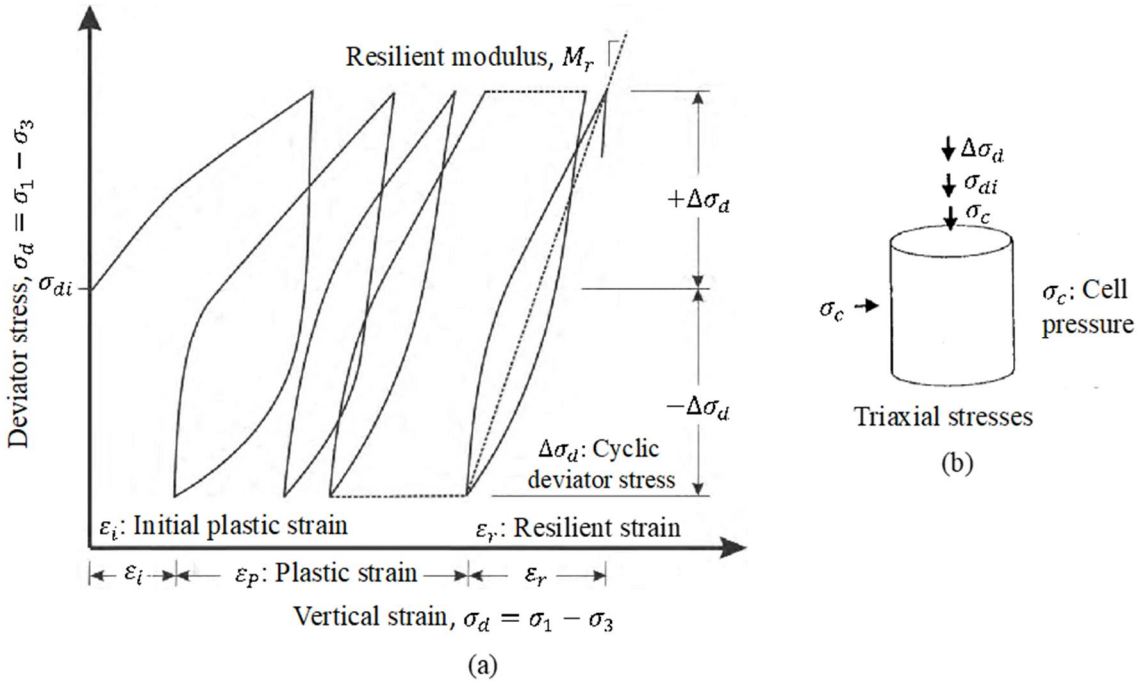

Figure 4: Cyclic loading under triaxial conditions (a) stress-strain relationship; (b) free body diagram of sample in triaxial apparatus (adapted from Selig and Waters, 1994)

The *magnitude* of cyclic loading defined in triaxial stress space consists of the confining stress (σ_c), initial deviator stress (σ_{di}) and cyclic deviator stress ($\Delta\sigma_d$) as highlighted in Figure 4(a) and Figure 4(b). The confining stress represents the effect of the seating pressure and overburden pressure which remain constant during cyclic loading. The initial deviator stress which represents the midpoint of a single loading cycle is calculated from Equation (4). The cyclic deviator stress which oscillates about the initial deviator stress is calculated from Equation (5). The maximum and minimum vertical stresses in Equations (4) and (5) can be obtained from field measurements or calculated via computer modelling (i.e.: finite element analyses) with a loading pattern as shown in Figure 3.

$$\sigma_{di} = (\sigma_{max} + \sigma_{min})/2 \quad (4)$$

$$\Delta\sigma_d = (\sigma_{max} - \sigma_{min})/2 \quad (5)$$

Where:

σ_{di} = initial deviator stress,

$\Delta\sigma_d$ = cyclic deviator stress,

σ_{max} = maximum vertical stress,

σ_{min} = minimum vertical stress.

The *frequency* (f) of cyclic loading represents the duration of a single load application as a direct result of the speed of a passing train. The frequency depends primarily on the operating speed and influence length as represented in Equation (6). The influence length is the distance between zero stresses or

strains experienced by a soil element subjected to a load application based on the loading pattern shown in Figure 3.

$$f = V / L \tag{6}$$

Where:

V = train speed,

L = influence length.

In this study, the cyclic loading was characterized through finite element modelling using a software package called ABAQUS where a multi-layer linear elastic model was developed. The choice of a linear elastic model was based on the fact that only the magnitudes of the stresses and not the strains acting on a railway foundation were of interest to be used as input parameters in the laboratory tests. The track structure and material properties were representative of a conventional railway foundation in South Africa for transportation of freight. The track structure which is depicted in Figure 5 consisted of 60 kg/m rails at a gauge of 1065 mm, PY prestressed concrete sleepers spaced at 650 mm center-to-center and a ballast depth of 300 mm, subballast layer of 200 mm and subgrade layer of 2800 mm. The mesh structure of the model consisted of 187 050 elements and 197 762 nodes and the track length was 20 m with 31 sleepers as shown in Figure 5. The three-dimensional model was meshed using eight node linear hexahedron elements with full integration of the average strain in each element. Due to the triangular shape of the ballast profile, wedged hexahedron elements were used in the ballast layer with tie condition to the subballast layer for continuity. The material properties used as input parameters in the model are shown in Table 1. Undrained conditions in the subballast and subgrade material were modelled with a Poisson's ratio of 0.49 (Potts and Zdravkovic, 1999). The configuration of the representative wagons used in the model is shown in Figure 6 where the critical spacing of the axles was taken as the four closest axles. The loading and boundary conditions of the model are depicted in Figure 7. The boundary conditions were chosen in which a way that they do not influence the point of interest, which is at the center of the model, where displacements were allowed in the x, y and z axis.

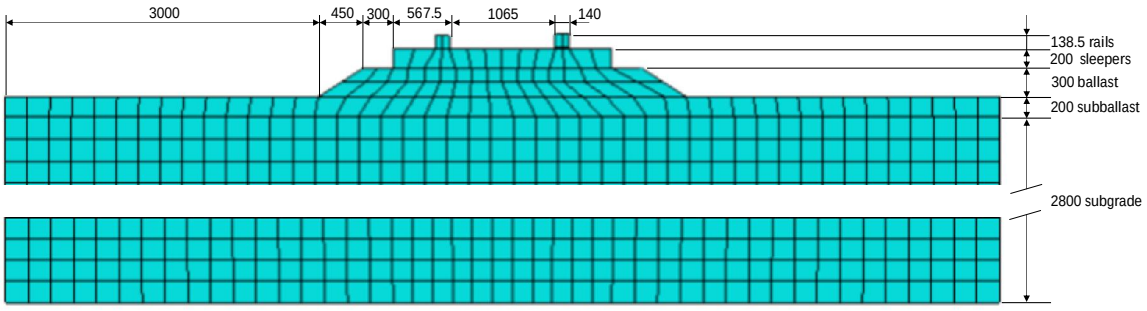

Figure 5: Track and mesh structure for finite element model (dimensions in mm, not drawn to scale)

Table 1:Material properties of the track structure

Track component	Young's Modulus (MPa)	Poisson's ratio	Density (kg/m^3)
Rails	205 000	0.30	7850
Sleepers	34 000	0.30	2400
Ballast (300 mm depth)	200	0.35	1800
Subballast (200 mm depth)	120	0.49	2000
Subgrade (3000 mm depth)	100	0.49	2000

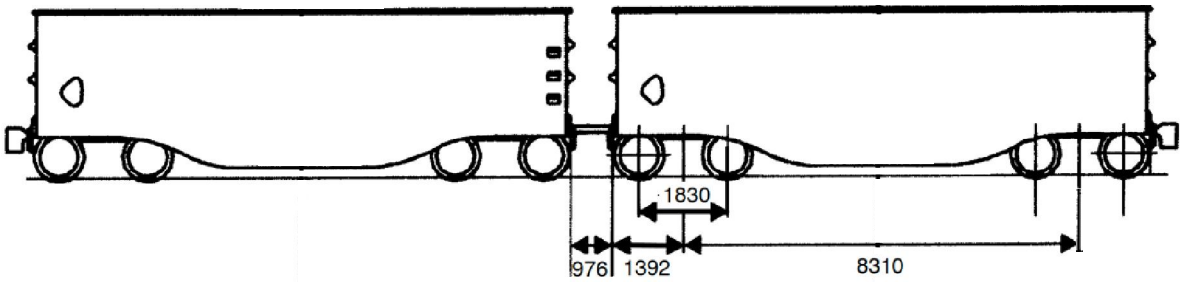

Figure 6: Representative wagons and the spacing of critical axles (dimensions in mm)

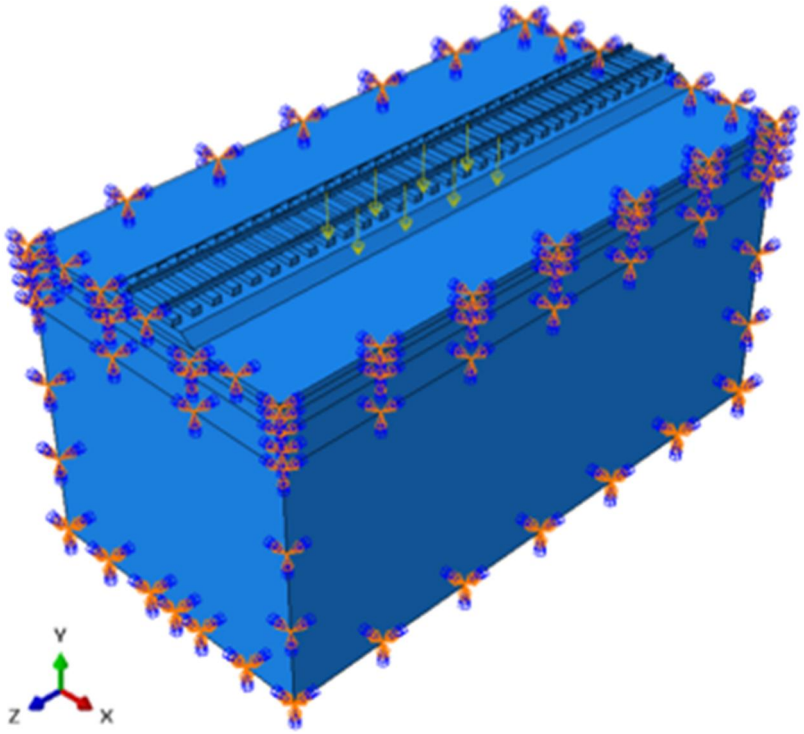

Figure 7: Loading and boundary conditions of finite element model

The typical results of the vertical stresses obtained from the finite element analysis taken from the 20 tonnes per axle loading case are shown in Figure 8. The graphs of the stress distribution on the subballast and subgrade layers are depicted in Figure 9. The magnitudes of the stresses in Figure 9 have been

normalized such that all the axle loading cases for each layer can be represented by one graph. With reference to the y-axis, the top of the subballast layer is located where the maximum vertical stress is -7.129 × 10^4 N/m^2, normalized to -3.56 kPa per tonne. The top of the subgrade layer is located below the subballast where the maximum vertical stress is -4.639 × 10^4 N/m^2, normalized to -2.32 kPa per tonne.

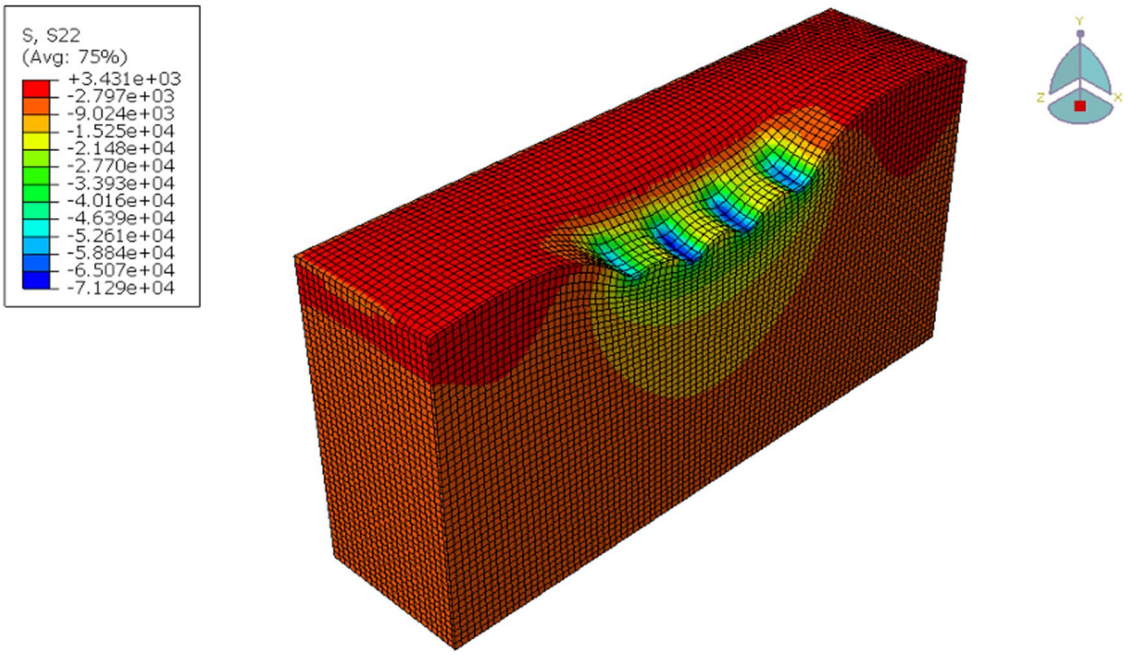

Figure 8: The vertical stress results from finite element model (note: units of stress in N/m^2, negative stress indicates compression)

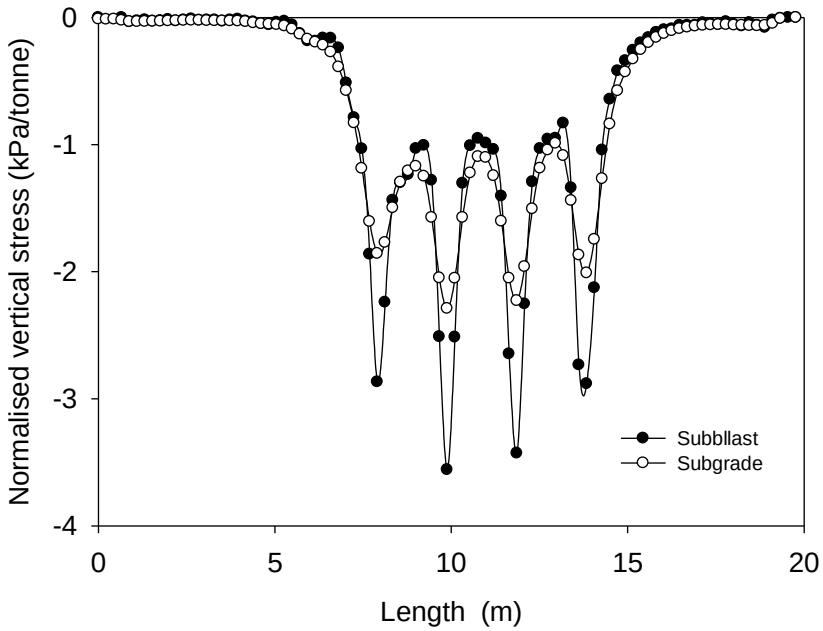

Figure 9: Vertical stress distribution for subballast and subgrade material

The magnitudes of cyclic loading are populated in Table 2. The initial deviator stress and cyclic deviator stresses for each axle loading case were calculated using Equation (4) and (5) together with Figure 8 and Figure 9. The maximum vertical stress was taken at a length of 10 m and the minimum vertical stress at a length of 0 m and 20 m. The cyclic loading frequency was calculated using Equation (3) for speeds ranging from 60 to 80 km/h with an influence length of 20 m. The calculated frequency for 60 km/h speed was 0.83 Hz and for 80 km/h speed was 1.11 Hz. For practical reasons for the laboratory testing, a fixed frequency of 1.00 Hz was adopted for all axle loading cases and materials.

Table 2: Characterization of cyclic loading for the subballast and subgrade material

Axle loading (tonnes)	**Subballast material**		**Subgrade material**		**Frequency (Hz)**
	Initial stress (kPa)	**Cyclic amplitude (kPa)**	**Initial stress (kPa)**	**Cyclic amplitude (kPa)**	
20.0	41.7	35.7	33.6	23.6	1.0
26.0	52.4	46.4	40.7	30.6	
30.0	59.6	53.6	45.3	35.3	
32.5	64.0	58.0	48.3	38.3	
40.0	77.4	71.4	57.1	47.1	

5. EXPERIMENTAL WORK

5.1 Test materials

Two test materials which were representative of the subballast and subgrade material for a heavy-haul railway line in South Africa as specified by Transnet (2006) were used for the experiment. The particle size distribution of each material is shown in Figure 10. The physical properties of the test materials are populated in Table 3. Although both materials were classified as silty sands, the subballast material was composed of 75% sand particles, whilst the subgrade material was composed of 67% sand particles. The plasticity index was 3% and 9% for the subballast and subgrade material, respectively.

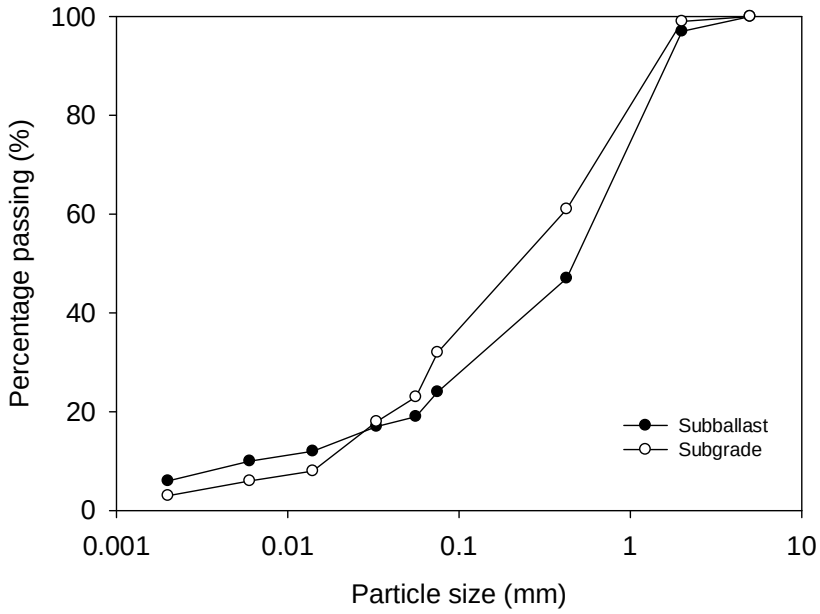

Figure 10: Particle size distribution of test materials

Table 3: Physical properties of the test materials

Material Property	**Subballast**	**Subgrade**
% gravel	2	1
% sand	75	67
% silts	18	29
% clay	5	3
Description	Silty sand	Silty sand
Liquid limit (%)	17	25
Plastic limit (%)	20	34
Plasticity index (%)	3	9
Linear shrinkage (%)	2	4
Specific gravity	2.89	2.64
Grading modulus	1.30	1.09

5.2 Test equipment

A double walled cyclic triaxial apparatus manufactured by GDS Instruments Ltd. (Hook, United Kingdom) which was developed by the University of Pretoria for this study is shown schematically in Figure 11 and photographically in Figure 12. The triaxial cell consists of a glass wall which separates the outer and inner cells. For saturated conditions, the triaxial cell can be operated as a single cell. For unsaturated conditions, the triaxial cell can be operated as a double cell, where the pressure in the outer cell and inner cell are controlled independently in order to measure the total volume change as described by Wheeler (1988). A complimentary method which can be used for measuring the total volume change involves the use of local instrumentations as described by Clayton & Khatrush (1986). The system consists of three pressure controllers, each with a maximum pressure of 2000 kPa to measure and

control the cell pressure and pore water pressure. The system is equipped with three pressure transducers to measure the pressure across the outer and inner cell and the pressures at the base and top of the sample. A pneumatic pressure controller can be used to impose pore air pressure into the sample in order to introduce matric suction by means of axis-translation for testing at unsaturated soil conditions. The axial load is measured by means of a load cell connected to the top cap by a suction sleeve. The cyclic loading is controlled by a loading ram connected to a brushless DC servo-motor actuator fixed at the base of the cell. The maximum load and frequency of the actuator are 10 kN and 2 Hz, deliverable by means of load-, stress- and strain-controlled settings. The axial displacement is measured by a balanced ram platen with a 100 mm stoke. The ram is compensated for volumetric displacement of the loading ram in or out of the cell, such that the net volume change in the cell is zero. All components of the system are connected to a data-logger and a computer for system control, data acquisition and processing. A Nold-type deaerator is used to remove air from the testing water. The deaerator consists of an airtight 10-liter perspex reservoir, a motor-powered, fast rotating disk and a vacuum pump. The water tank is placed at 1 m above the triaxial cell to allow for gravity flow of water into the cell.

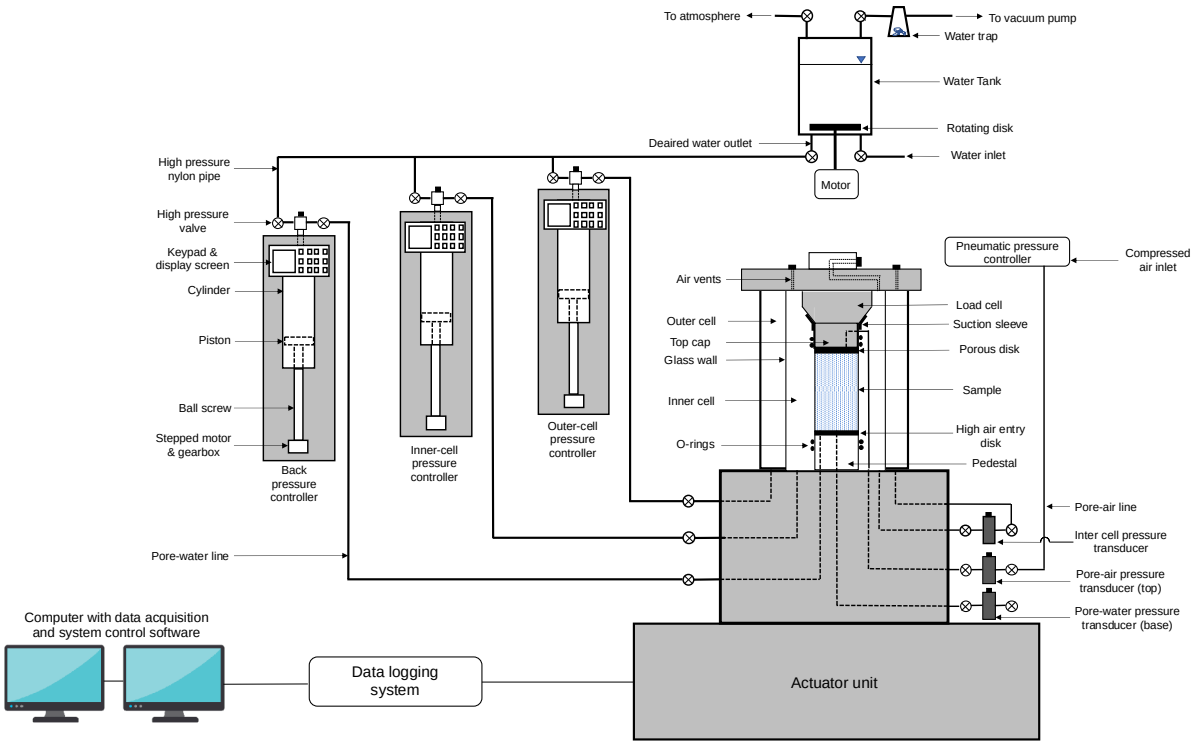

Figure 11: Schematic diagram of cyclic triaxial apparatus

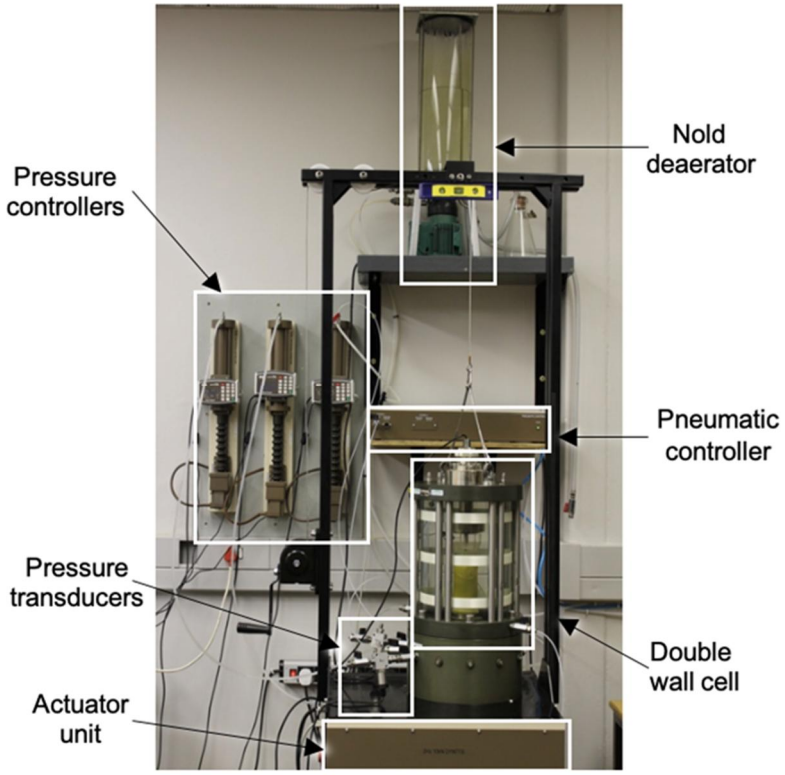

Figure 12: Photograph of cyclic triaxial apparatus

5.3 Test procedure

The test procedure which was carried out as part of the experimental work consisted of preparation of test materials, saturation, consolidation stage and monotonic stage and cyclic shear stage as shown in a diagram depicted in Figure 13. The details of the different test stages are given in the following paragraphs.

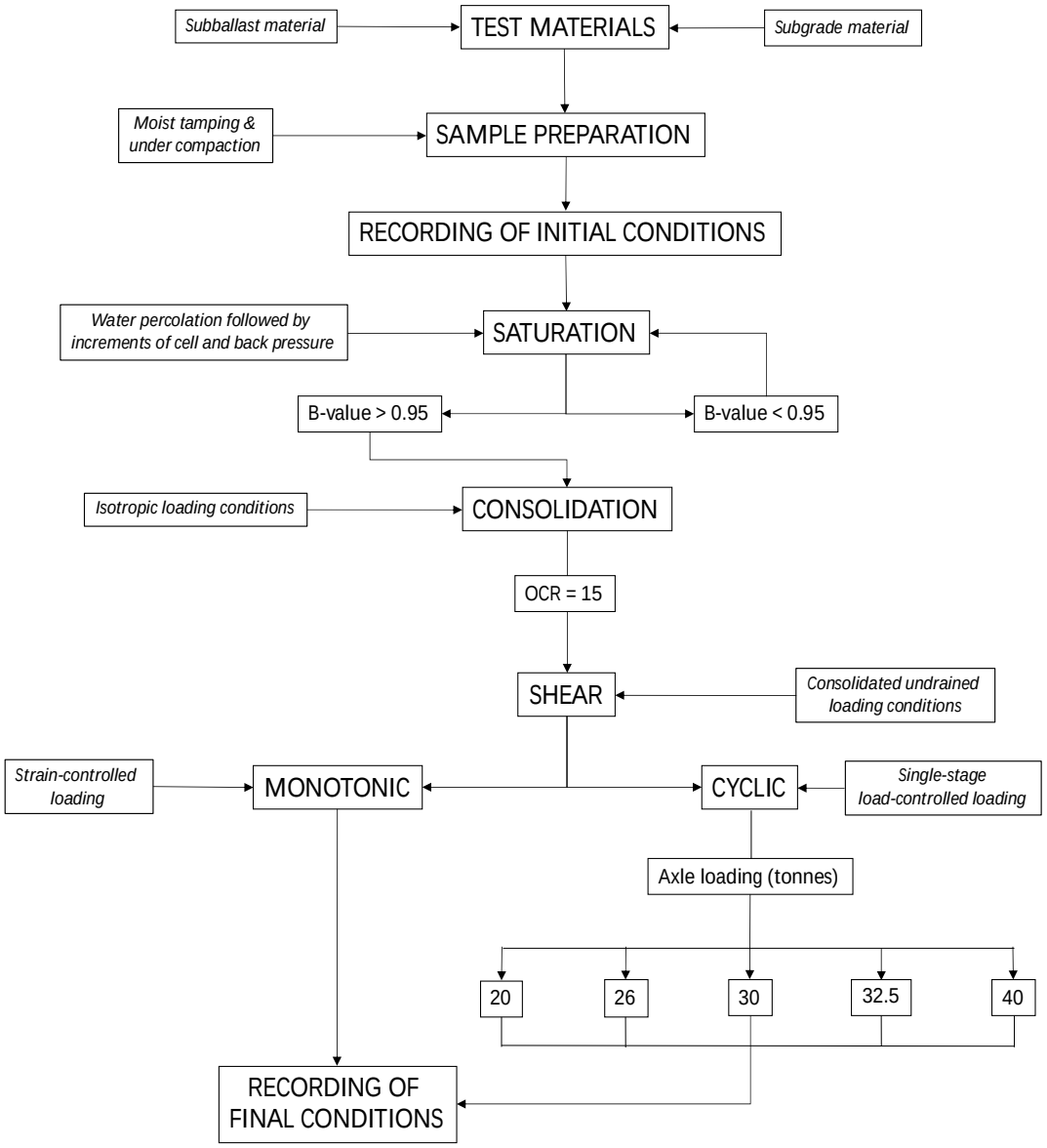

Figure 13: Test procedure and stages

5.3.1 Preparation and saturation of samples

Samples were prepared by means of moist tamping using under-compaction because Kuerbis and Vaid (1988) stated that moist tamping best reconstitutes the soil fabrics of compacted fills and Ladd (1978) stated that under-compaction results in a uniform density across the sample height. Samples were prepared at a specified target density and moisture content to ensure representation of the field conditions. Care was taken to prepare all samples to the same initial conditions. The initial conditions of the samples for the subballast and subgrade material are populated in Table 4 and Table 5, respectively. The samples were named according to material type and loading. SB and SG denotes the subballast and subgrade material, respectively. The number after SB or SG denotes the loading, where

00 represents monotonic loading, 20 represents 20 tonnes per axle, 26 represents 26 tonnes per axle and so forth.

Saturation of samples was achieved by means of percolation for 6 – 12 hours with deaired water charged with head pressure of 1 m, followed by the application of 50 kPa increments of back pressure and cell pressure as recommended by Black and Lee (1973). Saturation was achieved at a backpressure of 300 kPa. Full saturation was assumed to be achieved at minimum B-values of 0.95, calculated according to Equation (7) as specified by BS 1377. Final B-values for each sample for subballast and subgrade material are populated in Table 4 and Table 5, respectively.

$$B = (\Delta u_w)/(\Delta \sigma_c) \tag{7}$$

Where:

Δu_w = change in pore water pressure,

$\Delta \sigma_c$ = change in cell pressure.

Table 4: Initial conditions of subballast samples after preparation

Sample	Moisture Content	Bulk Density (kg/m^3)	Void Ratio	Final B-value
SB00	0.063	2202	0.381	0.967
SB20	0.061	2224	0.365	0.973
SB26	0.064	2206	0.379	0.955
SB30	0.063	2220	0.369	0.969
SB32.5	0.061	2212	0.372	0.975
SB40	0.062	2223	0.367	0.972

Table 5: Initial conditions of subgrade samples after preparation

Sample	Moisture Content	Bulk Density (kg/m^3)	Void Ratio	Final B-value
SG00	0.061	1806	0.552	0.974
SG20	0.064	1814	0.549	0.976
SG26	0.063	1830	0.534	0.971
SG30	0.061	1835	0.527	0.971
SG32.5	0.061	1792	0.563	0.979
SG40	0.064	1793	0.567	0.982

5.3.2 Consolidation stage

The objective of the consolidation stage was to replicate the effect of compaction in the field and introduce the state of heavily overconsolidation. Pressure plate measurements presented by Gräbe

(2002) obtained from a railway construction site indicated that the overconsolidation ratio of railway foundation materials is in the order of 15. As a result, all samples were isotopically consolidated with a cell pressure of 750 kPa and a back pressure of 300 kPa, followed by swelling back to a cell pressure of 330 kPa and a back pressure of 300 kPa. The results from the consolidation stage are presented in Section 6.1 of this paper.

5.3.3 Monotonic shear stage

The objective of the monotonic shear tests was to obtain the shear strength parameters needed to quantify the elasto-plastic model presented in Section 3 of this paper. The shear stage consisted of monotonic loading and cyclic loading. Undrained conditions were maintained as a representation of field conditions during loading. The axial load, pore water pressures and axial displacement were measured throughout the test. The back pressure and cell pressure were maintained at 300 kPa and 330 kPa, resulting in a mean effective stress of 30 kPa. Monotonic tests were conducted under strain control loading conditions to capture the peak strength (if present) at a strain rate of 0.05 % per minute as stated by Lade (2016). The results from the monotonic shear stage are presented in Section 6.2 of this paper.

5.3.4 Cyclic shear stage

The objective of the cyclic shear tests was to investigate the effect of increased axle loading on the behavior of railway foundation materials. Cyclic tests for the various axle loadings were conducted under load-control loading conditions. Shearing was conducted by means of single-stage loading, since some of the samples failed and multi-stage loading was not possible for all the axle loading cases. The cyclic loading applied to each sample was obtained from the results of the finite element modelling presented in Section 4 of this paper. A total number of load cycles of 2000 were applied because it represents the passage of 20 trains with 200 wagons without the dissipation of pore water pressures (i.e. undrained conditions), which is roughly the maximum possible number of trains per day. The results from the cyclic shear stage are presented in Section 6.3.

6. TEST RESULTS

6.1 Consolidation test

The results from the consolidation test are shown in Figure 14 (a) and (b) for the subballast and subgrade material, respectively. The consolidation properties are populated in Table 6. Both materials were

consolidated isotopically to an effective preconsolidation pressure of 450 kPa and swollen back to a mean effective stress of 30 kPa resulting in an overconsolidation ratio of 15.

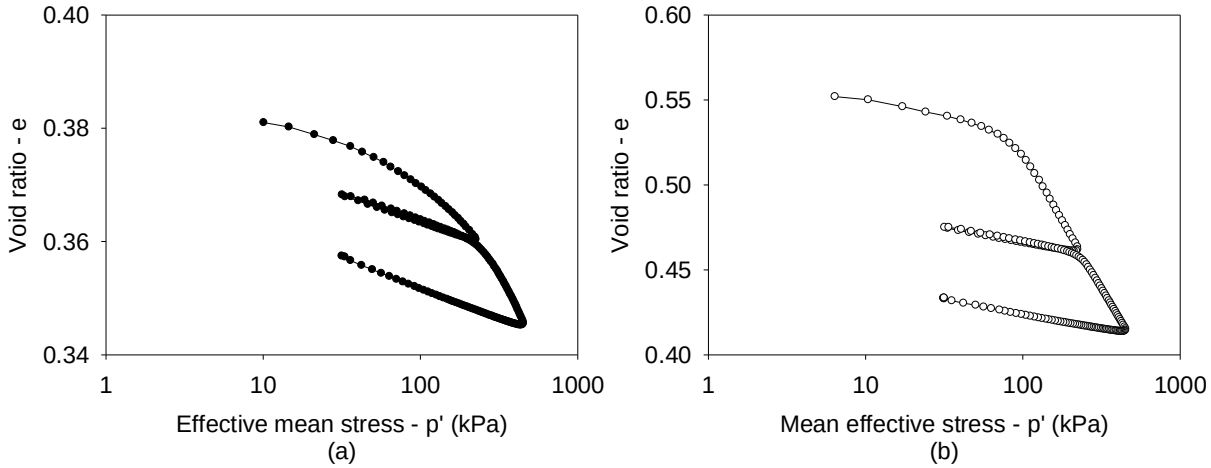

Figure 14: Typical isotropic consolidation of test materials: (a) subballast (b) subgrade.

Table 6: Isotropic consolidation parameters of test materials

Consolidation Parameter	**Subballast**	**Subgrade**
Slope of normal compression line: λ	-0.02	-0.06
Slope of unload-reload line: κ	-0.004	-0.007
Maximum consolidation pressure: p'_c (kPa)	450.0	450.0

6.2 Monotonic shear

The monotonic shear test results for the subballast and subgrade material are shown in Figure 15. Based on the effective stress ratio or excess pore water pressure, the critical states for both materials were reached after axial strain of 5%. The effective stress ratio at critical state for the subballast and subgrade material was taken as 1.5 and 1.2 respectively, as shown in Table 7. The development of negative excess pore water pressures as depicted in Figure 15 is indicative of dilation due to the heavily overconsolidated state.

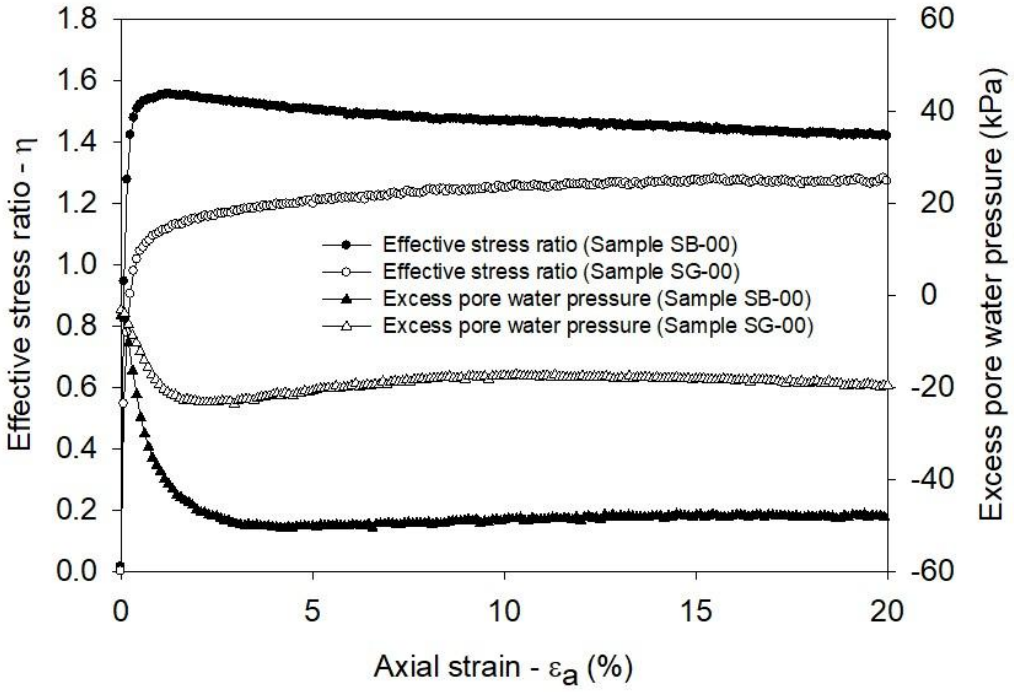

Figure 15: Monotonic shear behavior of test materials

Table 7: Shear strength parameters of test materials

Shear Strength Parameter	**Subballast**	**Subgrade**
Effective friction angle at the critical state: ϕ'_c (°)	36.9	30.0
Stress ratio at the critical state: M_C	1.50	1.20

6.3 Cyclic shear

The results from the cyclic shear tests are depicted in Figure 16, Figure 17 and Figure 18. The cyclic loading for each axle loading case of the subballast and subgrade material is shown in Figure 16 (a) and (b), respectively. The shape of the cyclic loading is consistent between the initial and final cycle in terms of the amplitude, pulses and peaks, thus deemed to be acceptable. The permanent strains of the subballast and subgrade material are shown in Figure 17 (a) and (b), respectively. The observable trend is that cyclic loading at low axle loading (i.e. 20 tonnes per axle) resulted in a linear accumulation of permanent strains, indicative of resilience and cycling at high axle loading (i.e. 40 tonnes per axle) resulted in an exponential accumulation of permanent strains, indicative of material failure. The resilient strains of the subballast and subgrade material are shown in Figure 18 (a) and (b), respectively. The observable trend is that the resilient strains decreased with initial cyclic loading, however, the decrease is greater at higher axle loadings, further indication of loss of resilience and material failure.

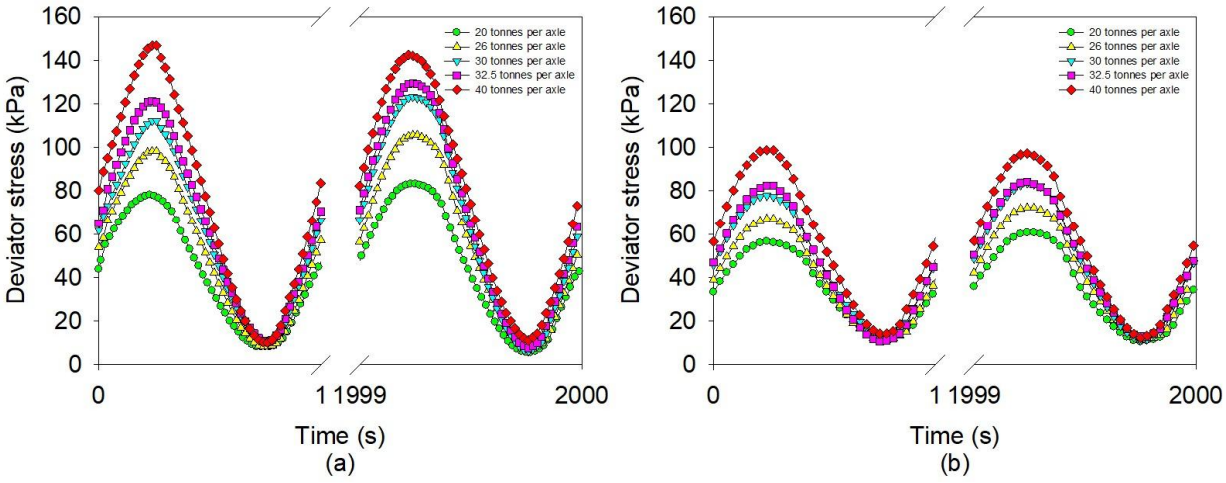

Figure 16: The cyclic loading on the (a) subballast and (b) subgrade material at various axle loading

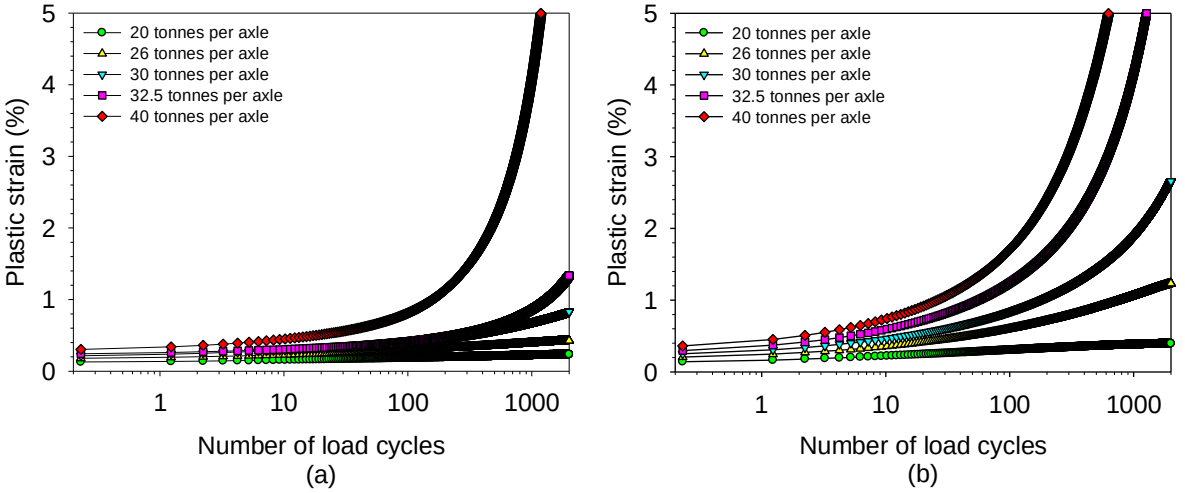

Figure 17: The permanent strain of (a) subballast and (b) subgrade material at various axle loading

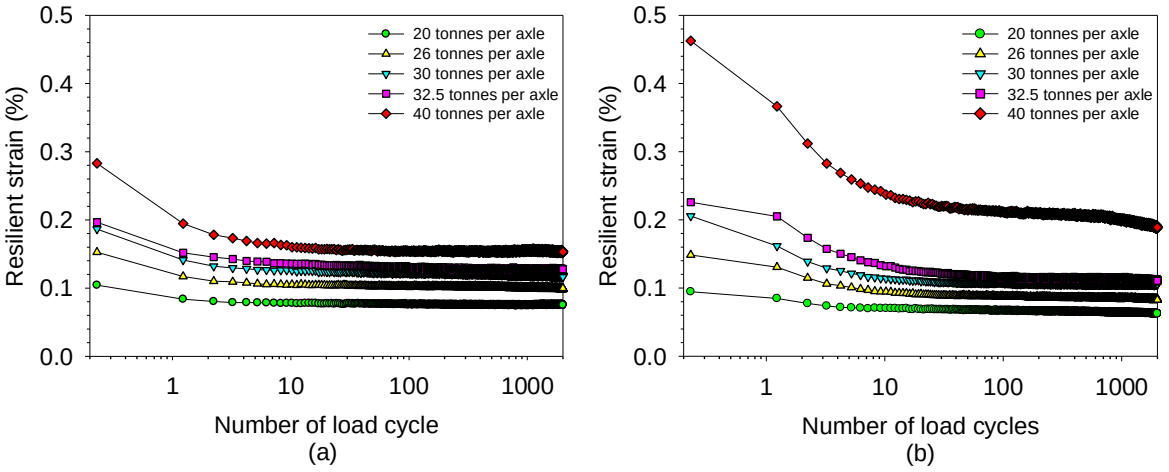

Figure 18: The resilient strain of (a) subballast and (b) subgrade material at various axle loading

7. DISCUSSION OF RESULTS

7.1 Effect of increased axle loading on the stress states and pore water pressures

The effect of increased axle loading on the stress states and excess pore water pressure was evaluated using elasto-plastic model and the pore water pressure line. The elasto-plastic state model is shown in Figure 19 (a) and the pore water pressure line is shown in Figure 19 (b). In the elasto-plastic model, the critical state lines and Roscoe curve were calculated based on Equations (1), (2) and (3). As a reminder, the critical state line and the Roscoe curve are stress state boundaries which separate the elastic and plastic behavior, where elastic behavior is expected below the stress state boundaries and plastic behavior is expected above or along the stress state boundaries. The excess pore water pressure line is represented by the excess pore water pressure measured during monotonic shear loading.

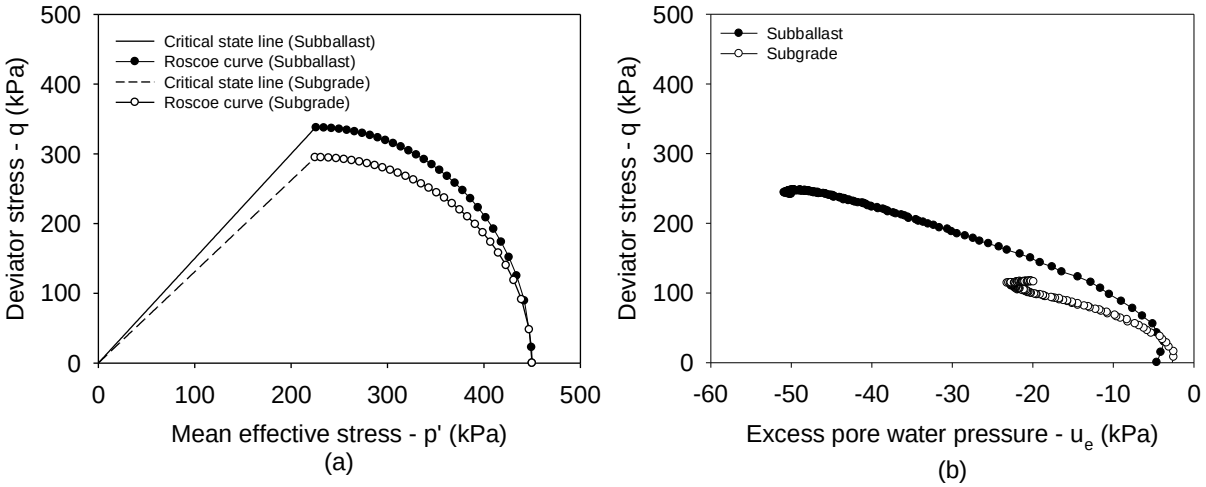

Figure 19: Quantification of the (a) elasto-plastic model and (b) pore water pressure line

The effect of increased axle loading on the stress states of the subballast and subgrade material is shown in Figure 20 and Figure 21, respectively. Each stress state point in the graphs represents the maximum deviator stress with the corresponding mean effective stress per load cycle. The common trend in all the samples is that the initial stress states resulted in dilation moving in the righthand direction. This was mainly caused by the initial heavily overconsolidated state of the samples. Samples whose initial stress states were above the critical state line resulted in a double-phase transition in soil behavior, from dilation to contraction and then work softening as indicated by the evolution of cyclic loading. This behavior occurred in the subballast material at 40 tonnes per axle (Figure 20) and in the subgrade material at 40, 32.5 and 30 tonnes per axle (Figure 21). Samples whose initial stress states were on the critical state line resulted in a single-phase transition in soil behavior, from dilation to contraction as indicated by the evolution of cyclic loading. This behavior occurred in the subballast material at 30 and 32.5 tonnes per axle (Figure 20) and in the subgrade material at 26 tonnes per axle (Figure 21). Samples

whose initial stress states were below the critical state line resulted in a no-phase transition in soil behavior and remained in dilation as indicated by the evolution of cyclic loading. This behavior occurred in the subballast material at 20 and 26 tonnes per axle (Figure 20) and in the subgrade material at 20 tonnes per axle (Figure 21). In conjunction with Figure 17 (a) and (b), it is evident that samples with exponential permanent strains were associated with a double-phase transition in soil behavior; those with a combination of exponential and linear permanent strains were associated with a single-phase transition in soil behavior; and those with linear permanent strains were associated with a no-phase transition in soil behavior. It can therefore be deduced that the failure mechanism of heavily overconsolidated railway materials due to increased axle loading is characterized mainly by a double-phase transition in soil behavior, where all stress states are situated above the critical state line. These results confirm the statement by Wood (1990) about the characteristic stress ratio model developed by Luong (1980a; 1980b) that the characteristic stress ratio line is related to the critical state line. The results presented in this study indicate that the phase-transition in soil behavior during cyclic loading is related to the critical state line where cyclic mobility occurred above the critical state line and shakedown occurred below the critical state line, which is in line with the characteristics stress ratio line developed by Luong (1980a; 1980b).

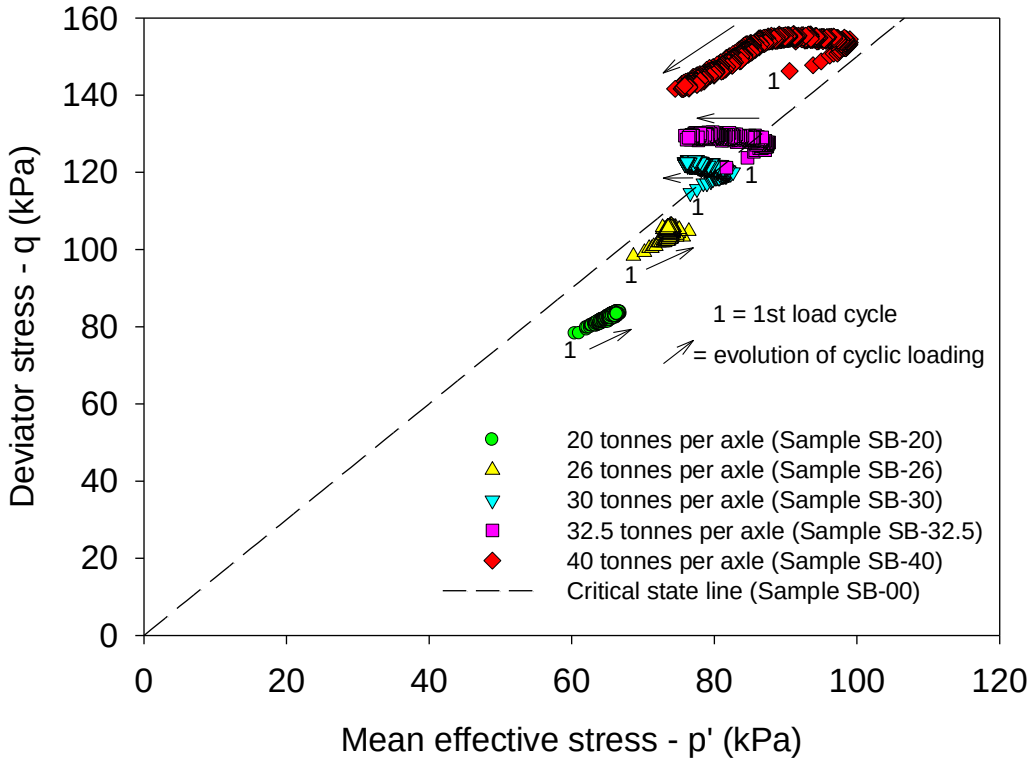

Figure 20: Effect of increased axle loading on the stress states of subballast material

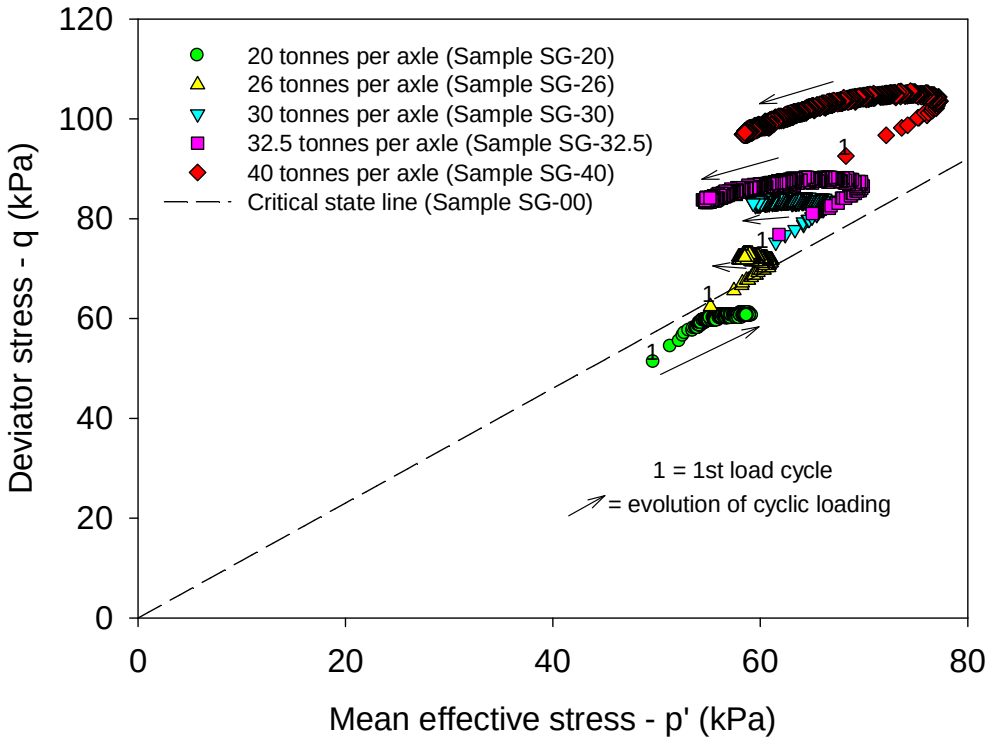

Figure 21: Effect of increased axle loading on the stress states of subgrade material

The effect of increased axle loading on the excess pore water pressures of the subballast and subgrade material is shown in Figure 22 and Figure 23, respectively. The negative excess pore water pressures during monotonic shear are indicative of dilation. From these results, it is evident that the phase transition in soil behavior was also present in the excess pore water pressures. However, the negative pore water pressures which developed during cyclic loading did not exceed the negative excess pore water pressures measured during monotonic loading. Furthermore, based on the development of the excess pore water pressures at cyclic loading of 40 tonnes per axle for both materials, the phase-transition in soil behavior does not seem to be directly related to the excess pore water pressure line.

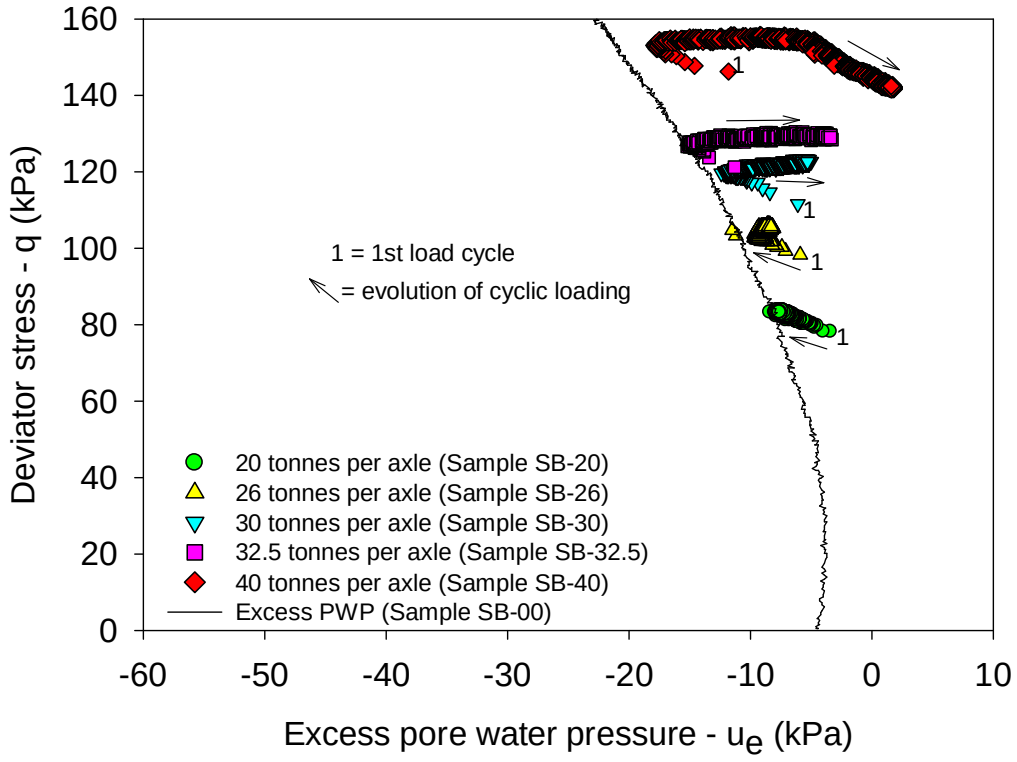

Figure 22: Effect of increased axle loading on the excess pore water pressures of subballast material

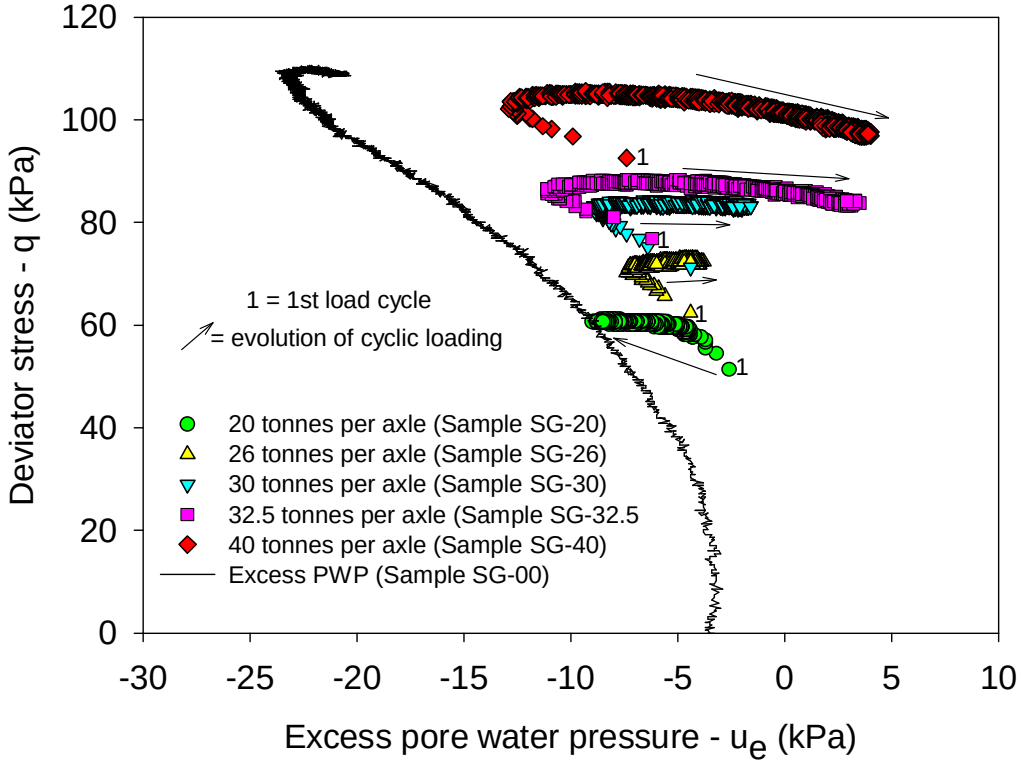

Figure 23: Effect of increased axle loading on the excess pore water pressures of subgrade material

7.2 Effect of increased loading on the permanent and resilient strain

The effect of increased axle loading on the permanent and resilient strain is shown in Figure 24 and Figure 25 for the subballast and subgrade material, respectively. Although, increased axle loading resulted in an increase in both the permanent and resilient strain, it is evident that a significant increase in the rate of permanent strain resulted in a decrease in the rate of the resilient strain. This is noticeable between 32.5 and 40 tonnes per axle for the subballast material depicted in Figure 24 and between 30 and 32.5 tonnes per axle for the subgrade material depicted in Figure 25. The opposite is also true, where an increase in the rate of resilient strain resulted in a decrease in the rate of the permanent strain between 32.5 and 40 tonnes per axle as depicted in Figure 25. In response to increased axle loading, it can therefore be said that the rate of increase of the resilient strain is inversely related to the rate of increase of the permanent strain. These results confirm the philosophy stated by Li and Selig (1996) that the excessive cumulative permanent strain is indicative of railway foundation failure which is seen to be associated with decreased resilience. These results also confirm the statement maintained by Gräbe and Clayton (2014) that the response of a well-designed flexible pavement will be largely resilient with almost all the deformations recoverable.

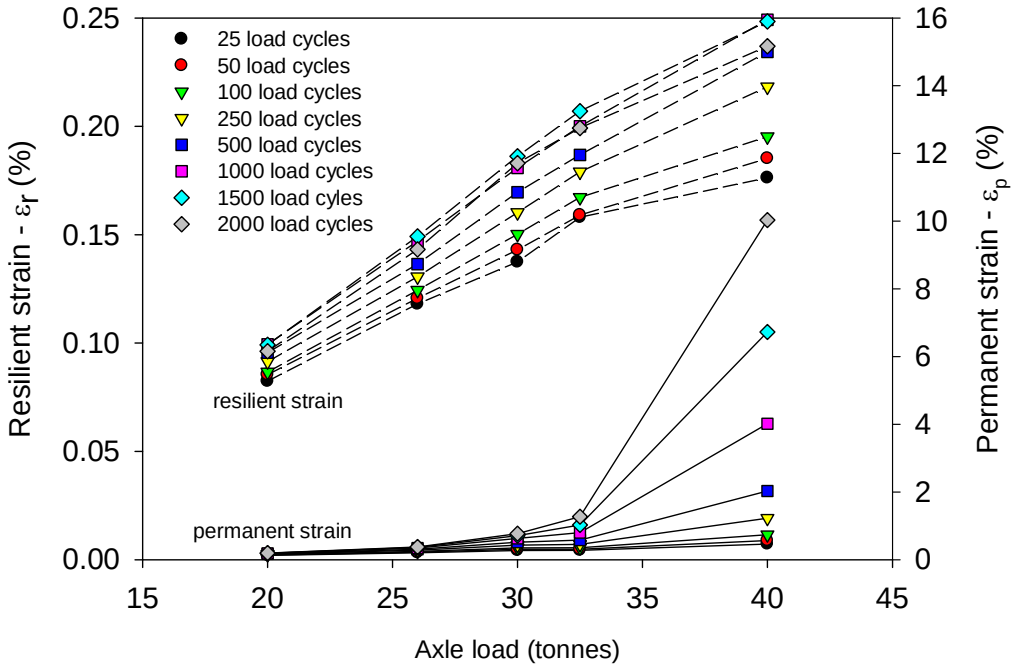

Figure 24: Effect of increased axle loading on the resilient and permanent strain of subballast material

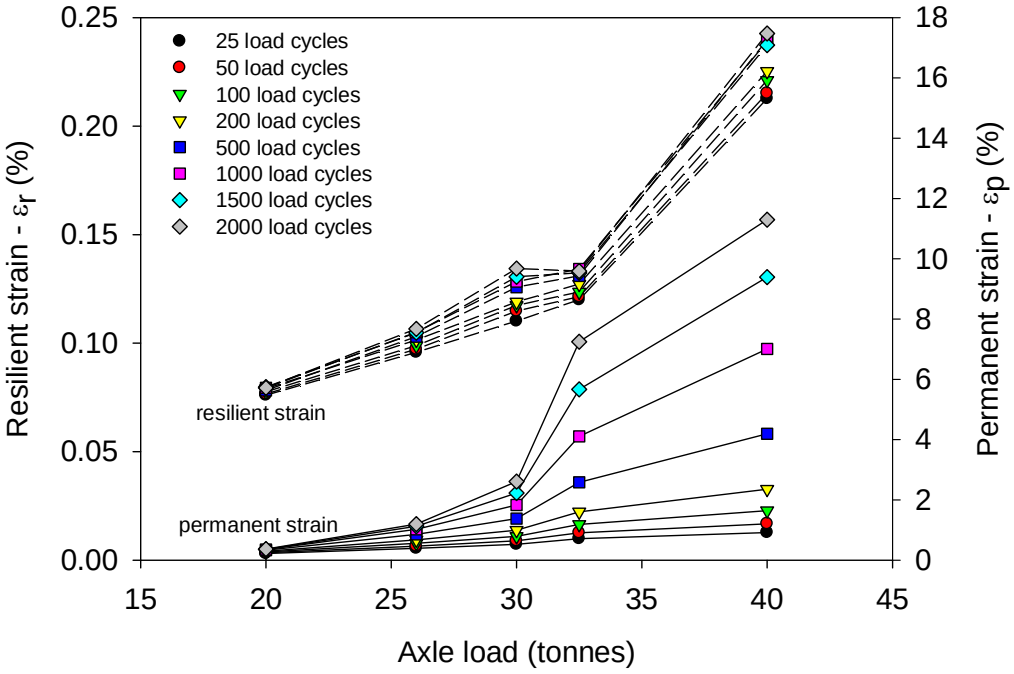

Figure 25: Effect of increased axle loading on the resilient and permanent strain of subgrade material

8. CONCLUSION

The objective of this study was to investigate the effect of increased axle loading on the behavior of heavily overconsolidated railway foundation materials. The methodology followed involved undertaking a literature study; presentation of an elasto-plastic theoretical model for evaluating the soil behavior; characterization of cyclic railway loading via finite element analysis, experimental work in the laboratory using a cyclic triaxial apparatus and detailed analyses, interpretation and discussion of the test results. Based on the test results, the following conclusions were reached:

- The critical state line from the elasto-plastic model was found to be related to the phase-transition in soil behavior and
- The permanent strain was found to be inversely related to the resilient strain, where an increased rate of the permanent strain resulted in a decreased rate of the resilient strain and vice versa.

In relation to the effect of increased axle loading on the behavior of heavily overconsolidated railway foundation materials, it can therefore be concluded that resilience is characterized by a no-phase transition in soil behavior coupled with consistent dilation predominated by resilient strains and shakedown while failure is characterized by a double-phase transition in soil behavior evolving from dilation to contraction and then work softening predominated by permanent strains and cyclic mobility. Lastly, for the purpose of design and maintenance of railway foundations, materials which exhibit

double-phase transition in soil behavior should be avoided as they were found to be prone to contraction, softening and material failure with excessive permanent deformations.

9. ACKNOWLEDGEMENTS

The University of Pretoria and Transnet Freight Rail are greatly acknowledged for their technical and financial support towards this research.

REFERENCES

Atkinson JH, Bransby PL. The mechanics of soils. Berkshire: McGraw-Hill Book Company; 1978.

Black DK, Lee KL. Saturating laboratory samples by back pressure. ASCE J. Soil Mech & Found Div. 1973;99:75-93.

BS 1377. Methods for test for soils for civil engineering purposes. London: British Standards Institution; 1990.

Clayton CRI, Khatrush SA. A new device for measuring local strains on triaxial specimens. Geotechnique. 1986;36:593-7.

Cole C. Longitudinal train dynamics. In: Iwnicki E, editors. Handbook of railway vehicle dynamic. Boca Raton: Taylor & Francis Group; 2006. p. 239- 77.

Gräbe PJ, Resilient and permanent deformation of railway foundations under principal stress rotation [PhD thesis]. Southampton: University of Southampton; 2002.

Gräbe PJ, Clayton CRI. Effects of principal stress rotation on permanent deformation in rail track foundations. ASCE J. Geotech & Geoenviron Eng. 2009. 135:555-65.

Gräbe PJ, Clayton CRI. Effects of principal stress rotation on resilient deformation in rail track foundation. ASCE J. Geotech & Geoenviron Eng. 2014;140: https://doi.org/10.1061/(ASCE)GT.1943-5606.0001023

Hay WW. Railway Engineering. 2nd ed. New York: John Wiley & Sons; 1982.

Korpanec I, Rebeyrotte E, Guigon M, Tordai L. Increasing axle load in Europe. Proc 8th Int Heavy Haul Conf. 2005 June 14-16; Rio de Janerio. Companhia Vale do Rio Doce; 2005. p. 227-35.

Kuerbis RH, Vaid YP. Sand sample preparation. Soils and Foundations. 1988;28:107-18.

Ladd RS. Preparing test specimens using undercompaction. Geotechnical Testing J. 1978;1:16-23.

Lade PV. Triaxial testing of soils. West Sussex: John Wiley & Sons; 2016.

Li D, Hyslip J, Sussmann T, Chrismer S. Railway geotechnics. New York: Taylor & Francis Group; 2016.

Li D, Selig ET. Resilient modulus for fine-grained subgrade soils. ASCE J Geotech Eng. 1994;120:939-957.

Li D, Selig ET. Cumulative plastic deformation for fine-grained subgrade soils. ASCE J Geotech Eng. 1996;122:1006-13.

Li D, Selig ET. Method for railroad track foundation design I: development. ASCE J Geotech & Geoenv Eng. 1998a:124(4):316-22.

Li D, Selig ET. Method for railroad track foundation design I: applications. ASCE J Geotech & Geoenviron Eng. 1998b;124(4):323-29.

Luong MP. Phénmoènes cycliques dans les sols pulvérulents. Revue Française de Géotechnique. 1980a;10:39-49.

Luong MP. Stress-strain aspects of cohesionless soils under cyclic and transient loading. Proc Int Sym of Soils under Cyclic & Transient Loading; 1980 Jan 7-11; Rotterdam. The Netherlands: Balkema; 1980b. p. 315-24.

ORE. The dynamic effects due to increasing axle loads from 20 to 22.5 tonnes and the estimated increase in track cost maintenance. Utrecht: The Netherland; 1987;4:1-49.

O'Reilly MP, Brown SF. Cyclic loading in geotechnical engineering. In: O'Reilly M, Brown SF, editors. Cyclic loading of soils. London: Blackie & Sons; 1991. p.1-19.

Potts DM, Zdravkovic L. Finite element analysis in geotechnical engineering: theory. London: Thomas Telford Ltd; 1999.

Powrie W, Yang L, Clayton CRI. Stress changes in the ground below ballasted railway track during train passage. Proc Inst Mech Eng. J Rail & Rapid. 2007;221(2):247-262.

Priest JA, Powrie W, Yang L, Gräbe PJ, Clayton CRI. Measurement of transient ground movements below a ballasted railway line. Geotechnique. 2010;60(9):667-677.

Roscoe KH, Burland JB. On the generalised stress-strain behavior of 'wet' clay. Proc Euro Conf Soil Mech & Found Eng. 1968;1:47-54.

Selig ET, Waters JM. Track geotechnology and substructure management. London: Thomas Telford; 1994.

Transnet. Specification for Railway Earthworks S410. 2006 March. pp.1-16

Wheeler SJ. The undrained shear strength of soils containing large gas bubbles. Geotechnique. 1988;38:399-413.

Wood D. Soil behavior and critical state soil mechanics. Cambridge: Cambridge University Press; 1990.